Intraskeletal Osteohistovariability Reveals Complex Growth Strategies in a Late Cretaceous Enantiornithine

Jessie Atterholt[1,2]*, Ashley W. Poust[2,3], Gregory M. Erickson[4] and Jingmai K. O'Connor[5]

[1]Graduate College of Biomedical Sciences, Western University of Health Sciences, Pomona, CA, United States, [2]University of California Museum of Paleontology, Berkeley, CA, United States, [3]San Diego Natural History Museum, San Diego, CA, United States, [4]Department of Biological Science, Florida State University, Tallahassee, FL, United States, [5]Field Museum of Natural History, Chicago, IL, United States

Most crown-birds experience rapid growth, reaching adult size within a year. Rapid growth strategies evolved within Aves multiple times during the Cretaceous, documented in the Confuciusornithiformes and the Ornithuromorpha. In contrast, osteohistological data suggest the Enantiornithes, the dominant clade of Cretaceous terrestrial birds, were characterized by much slower growth rates that were sustained longer into adulthood. Here we provide evidence for a unique growth strategy involving relatively rapid growth in the Late Cretaceous avisaurid enantiornithine, *Mirarce eatoni*. Multiple appendicular skeletal elements were sectioned for osteohistological analysis. These show remarkable intraskeletal variation, and high levels of variation even between individual sections. The radius is composed of parallel-fibered bone, similar to histological descriptions in other enantiornithines. Other elements, in contrast, differ markedly from other members of the clade. The humerus is composed of parallel-fibered bone with a middle layer of incipient fibrolamellar bone and several growth lines in the outer circumferential layer and near the endosteal border. The endosteal and periosteal layers of slow-growing bone indicate cyclical variation in growth rates. The femur shows regions of coarse compact cancellous bone and parallel-fibered bone with numerous secondary osteons, and only a single growth line. The tarsometatarsus is predominantly fibrolamellar in texture, with several asymmetrical growth lines located throughout the cortex; this element exhibits strong cortical drift. Growth lines in both the endosteal and periosteal portions of the cortex indicate that, like the humerus, growth rates of this bone varied cyclically. The two phalanges studied here are composed of parallel-fibered bone with extensive evidence of and remodeling over possible regions of coarse compact cancellous bone. Although *Mirarce* is one of the largest known enantiornithines, slow and protracted growth documented in similarly-sized taxa suggests this bone texture is not merely a size-related scaling effect. These findings indicate that by the Late Cretaceous, some enantiornithines had evolved absolutely higher growth rates and more complex life history strategies, in which growth rates varied across the skeleton. Furthermore, a variety of strategies were employed to achieve adult size and morphology, including cycles of slow and fast growth, asymmetrical growth within a single element, and extensive remodeling.

Keywords: histology, mesozoic birds, enantiornithine, growth, life history evolution

INTRODUCTION

When, how, and why the derived rapid growth strategy that characterizes most modern birds evolved in Aves and the Dinosauria is of intense interest to evolutionary biologists (Chinsamy-Turan, 2005; Erickson et al., 2009; Xu et al., 2014; O'Connor et al., 2018). Living birds nearly all reach skeletal maturity within the first year, some achieving adult size in only a matter of weeks (Gill, 2007; Bourdon et al., 2009). In contrast, non-avian dinosaurs took several years to reach adult size, likely achieving reproductive maturity prior to skeletal maturity (Erickson et al., 2007; Lee and Werning, 2008). More rapid growth strategies, whereby skeletal maturity is achieved in a relatively shorter duration of time (here-within referred to simply as rapid growth), apparently evolved multiple times within Aves during the Cretaceous (Zheng et al., 2017; Chinsamy et al., 2020). Non-ornithothoracine stem avian lineages Jeholornithiformes, and Sapeornithiformes preserve lines of arrested growth (LAGs) in the cortex, and like the Archaeopterygidae and non-avian dinosaurs likely achieved reproductive maturity before skeletal maturity (Erickson et al., 2007; O'Connor et al., 2014; Zheng et al., 2014). A similar pattern has been inferred for the Enantiornithes, the dominant clade of Cretaceous land birds, and for early-diverging members of the Ornithuromorpha, the crown-ward clade that includes Neornithes (living birds) (O'Connor et al., 2014; Wang and Zhou, 2016). However, evidence suggests that the Early Cretaceous early-diverging pygostylian *Confuciusornis* evolved more rapid growth independent of and in parallel to the neornithine lineage (Zhang et al., 1998; De Ricqlès et al., 2003; Chinsamy et al., 2020). Similarly, although protracted growth strategies persisted in some Late Cretaceous lineages (Chinsamy et al., 1995), rapid growth evolved in the Ornithuromorpha ~128 Ma and possibly arose multiple times within this clade during the Early Cretaceous (O'Connor et al., 2015; Wang X.-R. et al., 2020). This information highlights the evolutionary lability of avian development.

Here we describe the long bone osteohistology of a large avisaurid enantiornithine, *Mirarce eatoni* (Atterholt et al., 2018), the holotype of which (and only known specimen) represents the most complete enantiornithine from North America. Given the relatively sparse global record of enantiornithines in the Late Cretaceous, this taxon stands to provide new insights into these enigmatic birds (O'Connor et al., 2011). Most post-cranial elements of *Mirarce* are preserved, including partial or complete representatives of all major limb bones, a pygostyle, and a partial sternum. All preserved elements show signs of somatic maturity, including compound bones that are completely fused and periosteal surfaces lacking substantial rugosity from incompletely formed primary osteons (Atterholt et al., 2018).

We describe the osteohistology from ground-sections of the humerus, radius, femur, third metatarsal, and two pedal phalanges–more elements than have been sampled in any previously studied enantiornithine bird, with the exception of the recent work on Early Cretaceous *Mirusavis* (Wang M. et al., 2020). This provides an opportunity to further explore intraskeletal histovariability in this clade. It is becoming increasingly common that anatomical descriptions include osteohistological data, and although this provides comparative material, these studies typically only sample just one or two elements (Zhang et al., 2013; Wang M. et al., 2014; Hu et al., 2015; Hu and O'Connor, 2017; Wang et al., 2017a). Recent research revealing high intraskeletal variability in bone tissue highlights the importance of studies utilizing greater numbers of bones whenever possible to facilitate interspecific comparisons between homologous elements (e.g., Horner et al., 2000; De Ricqlès et al., 2003; Woodward et al., 2014; Prondvai et al., 2018; Chinsamy et al., 2020; Cullen et al., 2020). As such, we sampled as many elements as permission allowed. Sampling was facilitated by the fact that, while the specimen is three-dimensionally preserved, it is disarticulated and partially fragmented, so minimally destructive samples could be taken along pre-existing breaks. Histological evidence from *Mirarce* indicates that intraskeletal variability is substantial in this taxon. The preserved bone tissue contributes to our understanding of growth strategies in the Enantiornithes and further elucidates the complex patterns of skeletal ontogeny in stem birds.

MATERIALS AND METHODS

Tissue samples from *Mirarce* were extracted from broken elements in order to minimize damage to the specimen, that at the time of sampling was undescribed. Samples were collected from near the mid-shaft diaphyses wherever possible. Because histological features are known to vary between elements (e.g., Horner et al., 1999; Erickson, 2005), samples were taken from five different bones: 1) a fragment from the cranial mid-shaft diaphysis of the right humerus (the left humerus remains completely intact); 2) a piece of the diaphysis of the right radius; 3) the proximal diaphysis of the right femur (the left femur remains completely intact); 4) a portion of the right metatarsal III extracted just proximal to the mid-diaphysis (the left tarsometatarsus is completely intact); and finally 5) two incomplete pedal phalanges (the 1st phalanx from pedal digit II and the 4th from pedal digit IV). The samples from the femur and phalanges represent entire cross sections of the elements, while those of the humerus, radius, and metatarsal represent only portions of their respective cortices. The holotype fossil skeleton and histological sections of *Mirarce* are housed in the University of California Museum of Paleontology, Berkeley, CA, United States (UCMP 139500).

All bone samples were embedded in the polyester resin Epothin (Buehler Ltd., Lake Bluff, IL) and sectioned into 1 mm wafers using a diamond-embedded saw (Isomet low-speed Saw, Buehler Ltd., Lake Bluff, IL). Wafers were mounted using epoxy (2-ton, Devcon, ITW Polymers Adhesives, Danvers, MA) on petrographic microscope slides and ground to
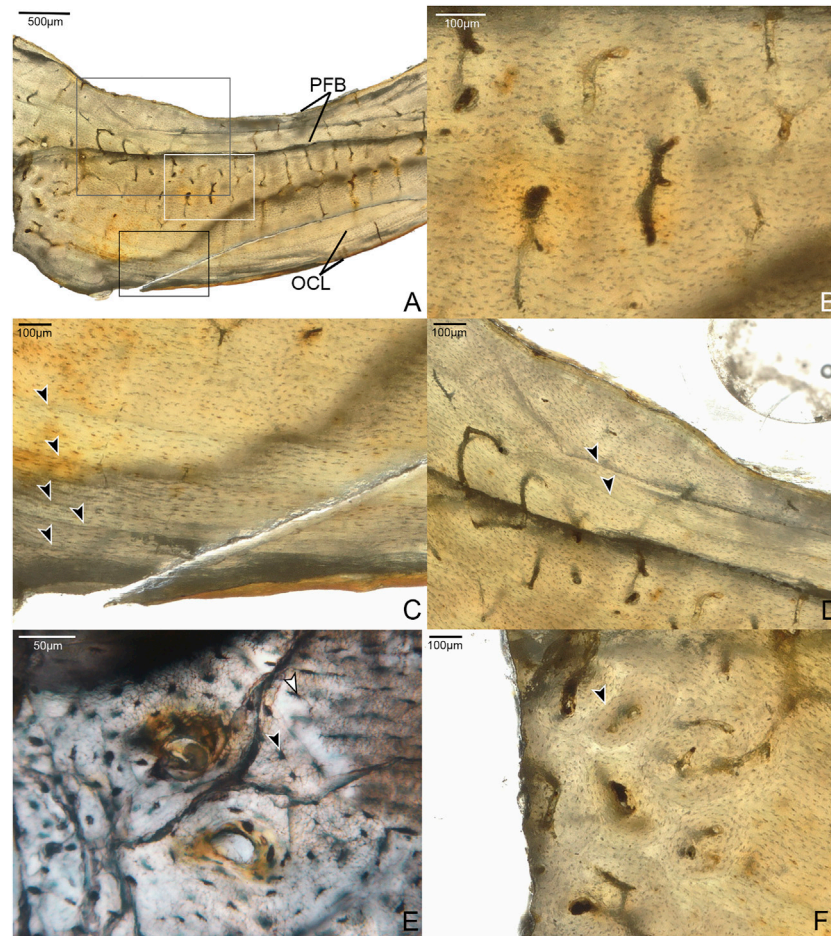
FIGURE 1 | Histological sections of the humerus of *Mirarce eatoni*. **(A)** Fragment of humeral cortex sectioned in this study, composed of a layer of parallel-fibered bone (PFB) and an outer circumferential layer (OCL) surrounding a middle layer of regional fibrolamellar bone and regions of simple vascular canals in woven bone; also, showing a series of LAGs near the periosteal margin, and a moderate level of vascular channels dominated by a reticular and/or radial patterning. 40x, plane light. **(B)** Section in white box of panel A; close-up of simple vascular canals in a region of weakly woven bone. 200x, plane light. **(C)** Section in black box of panel A; close-up of parallel-fibered OCL with growth lines indicated by arrows. 200x, plane light. **(D)** Section in gray box of panel A, showing the double endosteal growth line, separated into two separate lines transitioning from a LAG-like appearance to annulus-like. 100x, plane light. **(E)** Region of incipient fibrolamellar bone with developing primary osteons; image also shows details of cannaliculi, and differences in shape and size between osteons in woven bone (black arrow) compared to those in parallel-fibered regions (white arrow). 400x, plane light. **(F)** Region of fibrolamellar bone with mature osteons and some evidence of remodeling (secondary osteon, indicated by arrow). 200x, plane light.

approximately 100 µm thickness using a lap grinder (EcoMet 3, Buehler Ltd., Lake Bluff, IL) with descending grits (260–1,200) of silica-carbide grit paper using water as a lubricant. Slides were photographed using a Keyence VHX-7000 digital imaging microscope and a Nikon digital sight camera (Nikon Inc., Tokyo, Japan) tethered to a petrographic microscope (DS-U3 and DS-Fi2) and captured using the computer program NIS-Elements (Nikon Inc.). Sections were visualized under non-polarized light, linearly polarized light with crossed nicols, and with linearly polarized light with full waveplate compensation. The addition of a waveplate increases the color visibility of linear crystals, such as those of the bioapatite precipitated in vertebrate hard tissues. Under this view the additional colors are created by the orientation of the crystals such that orthogonally oriented fields retard the "slow" and "fast" components of light differently

and appear as opposing color gradients. No colors have been manipulated or altered digitally. Photos were edited in Adobe Photoshop CC (20.0.0; Adobe, San Jose, CA, United States). The terminology used to classify bone tissues follows the precedent of De Ricqlés (1976) and Francillon-Vieillot et al. (1990) as updated by Huttenlocker et al. (2013). Raw images are stored on Zenodo (https://zenodo.org).

All measurements were acquired using ImageJ (v.51; National Institute of Health, Bethesda, MD, United States). Cortical diameter (for complete cross-sections) was measured four times along different axes of the element in the transverse plane and averaged to generate a single figure representing this metric. Similarly, cortical thickness is reported as an average of six different measurements across the cortex (medially, laterally, cranially, caudally, and four midpoints

between these regions). Vascular area was calculated by manual outlining and measuring of each vascular pore observable in a given thin section. The total area of these spaces was then calculated and compared to the total cross-sectional area of an element to generate a percentage of vascular porosity.

RESULTS

Humerus

Fragments from the mid-shaft of the cortex of the broken left humerus of *Mirarce* were sectioned. The humeral samples have an average cortical thickness of 1542 μm. Two serial thin sections along the transverse plane of the element were made. Because this element is incomplete, our sampling does not capture the entire bone circumference. The cortex is composed primarily of parallel-fibered bone with regional incipient fibrolamellar bone and shows a thin, weakly-formed outer circumferential layer (OCL) (**Figure 1**). Although there is an endosteal layer of parallel-fibered bone, we do not interpret this as an inner circumferential layer (ICL) because there is no erosional boundary that separates it from the rest of the cortex, and it contains several vascular canals.

The element has mostly simple vascular canals, but developing primary osteons with lamellae in early stages of formation are present (**Figure 1E**). Regional fibrolamellar bone is identified based on areas of relatively high vascular porosity, and a primary matrix composed of randomly oriented woven bone. Because the osteons located in these regions of woven bone do not have distinct lamellae, and contain few osteocyte lacunae, these areas are interpreted as "incipient fibrolamellar bone" *sensu* Woodward et al. (2014). Such regional incipient fibrolamellar bone is also present in small areas of the humerus of adult enantiornithine STM 29-8 (O'Connor et al., 2014), though to a lesser extent than in *Mirarce*. This distinguishes these taxa from others in which the humeral diaphyseal cortices are completely composed of parallel-fibered bone (*Parvavis* IVPP V18586 (Wang M. et al., 2014), *Cruralispennia* IVPP V21711 (Wang et al., 2017b), and *Pterygornis* IVPP V16363 (Wang et al., 2017a)). In the humerus of *Mirarce*, minor remodeling is present, with several secondary osteons observed in the incipient fibrolamellar regions (**Figure 1F**).

There are at least six growth lines near the periosteal margin, although their precise number is obscured by numerous fine cracks in the outer region of the section. The innermost resembles an annulus, while the others are more distinctly formed and appear more like LAGs. Together, these structures corroborate inferences based on gross skeletal morphology that the individual was a somatically mature adult at the time of death (Atterholt et al., 2018).

There is also a growth line near the endosteal margin, that splits in two. Double LAGs (and even triple and quadruple) have been reported in other dinosaurs. Evidence suggests they are prevalent among theropods (e.g., Lee and O'Connor, 2013; Cullen et al., 2014; Evans et al., 2015; Cullen et al., 2020), and also occur in ornithischians (Werning, 2012), albeit more rarely. This is the first report of such a structure in an enantiornithine. In *Mirarce*,

one "branch" grades into a LAG-like distinct line and then transitions into a more annulus-like band of parallel-fibered bone, while the other simply trails off and fades into the surrounding cortical bone.

Vascularization is moderate, with channels concentrated in the middle of the cortex (in the regions of incipient fibrolamellar bone). The vascular canals are primarily longitudinally-oriented in one thin section, while radial and reticulating canals predominate in the consecutive thin section. This highlights the variability and disorganization of vascularity within this element (**Figure 1**). Such variability in canal orientation is unusual for enantiornithines, most of which show exclusively longitudinally-oriented vascularization (e.g., *Zhouornis* CNUVB-0903 (Zhang et al., 2013), STM 29-8 (O'Connor et al., 2014), *Eopengornis* STM24-1 (Wang X. et al., 2014), and *Parvavis* IVPP V18586 (Wang M. et al., 2014)). The areal density of vascular canals is moderate in the preserved portions of the cortex, comprising 4.2 and 1.1% of total cross-sectional area in the reticulated and longitudinally-dominated thin sections, respectively. This is generally higher than, but most similar to, *Zhouornis* CNUVB-0903 (vascular area of 1.57%) and an indeterminant enantiornithine taxon STM 29-8 (vascular area of 1.1%). This vascular area stands in stark contrast to that seen in other enantiornithine humeral sections (e.g., *Parvavis* IVPP V18586 (Wang M. et al., 2014), *Pterygornis* IVPP V16363 (Wang et al., 2017a), and *Cruralispennia* IVPP V21711 (Wang et al., 2017b)), that are nearly or completely avascular (**Table 1**).

Osteocyte lacunae are well-organized, although to a lesser degree in the incipient fibro-lamellar regions, and are extremely small (5–15 μm in length). Fine, intricate canaliculi are also well preserved, forming elaborate communications between neighboring lacunae (**Figure 1**). They differ moderately in shape through different portions of the cortex. In the OCL the osteocyte lacunae are extremely flattened. Within the rest of the cortex, they grade in morphology from rounded and disorganized in the more endosteal portion, where the bone matrix shows an incipient fibro-lamellar texture, to flatter and more organized in the outer half closer to the OCL where the tissue is parallel-fibered.

Radius

A small shard from the mid-shaft of the fragmented right radius was available for sectioning (**Figure 2**). The complete cortex is not captured, but some microstructural features can be discerned. An ICL is present, and at least a portion of the radius is composed of highly-cellular parallel-fibered bone, as inferred from the numerous osteocyte lacunae. This portion of the element also has very low vascularity. These sparsely-distributed canals are mainly simple (i.e., non-osteonal) and longitudinally oriented, although two incipient primary osteons are present (**Figure 2E**). Osteocyte lacunae are disorganized and bulbous relative to the lacunae in the humerus. No OCL is visible, however, the periosteal surface is not preserved in the fragment. One growth line is visible, in the mid-cortical portion of the preserved bone. Antebrachial elements that are composed entirely of slow-growing bone are also reported in the adult enantiornithine *Pterygornis* IVPP V16363 (Wang et al., 2017a) and subadults *Parvavis* IVPP V18586 (Wang M. et al., 2014) and

TABLE 1 | Summary of osteohistological attributes of *Mirarce eatoni* and select other enantiornithines.

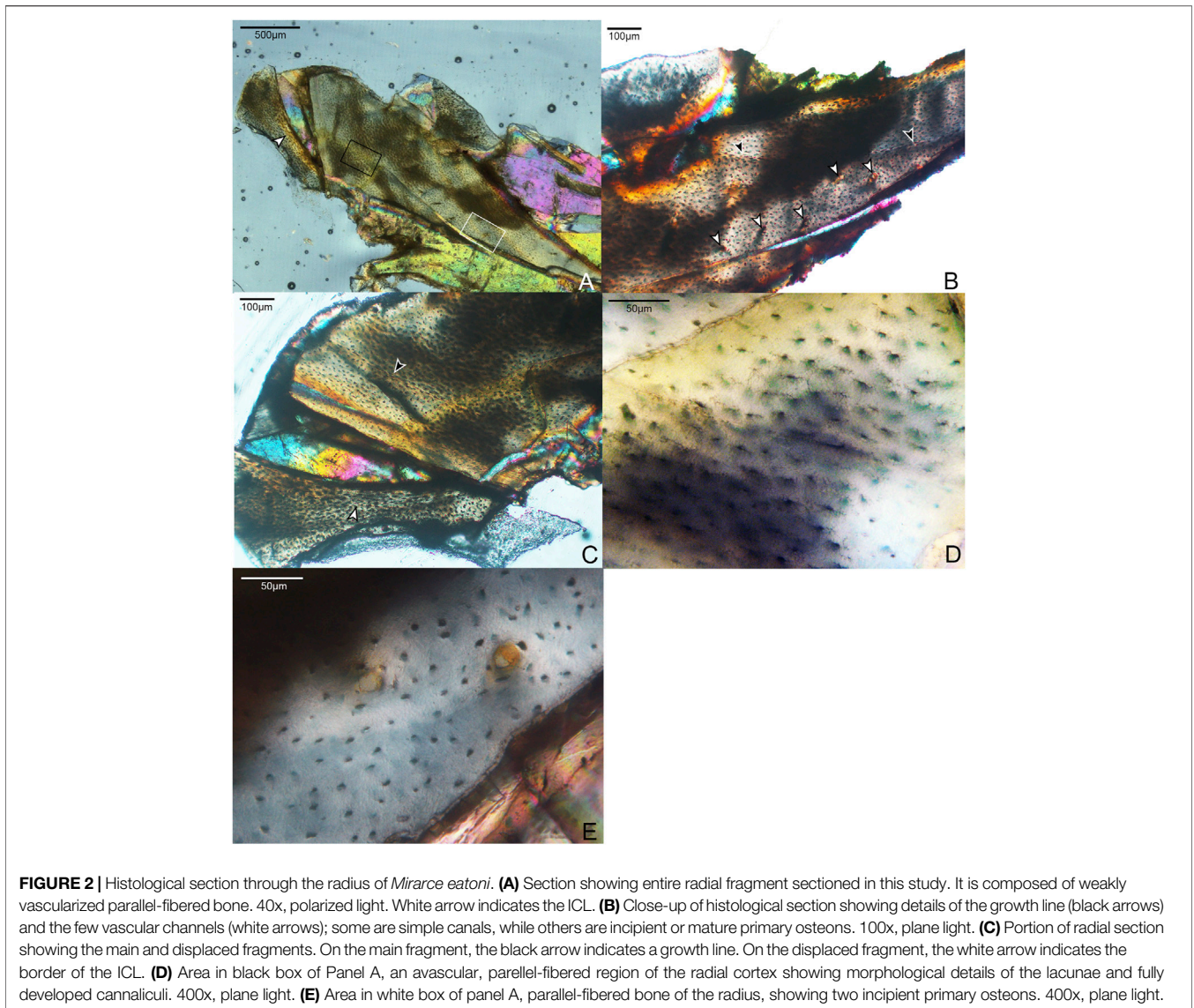| Taxon	Ontogenetic stage	Humerus	Ulna	Femur	Tarsometatarsus	DII, P1	DIV, PIV
Avimaia (IVPP V25371)	adult	—	—	0.1% 24.2† PFB GL: 1	—	—	—
Curalispennia (IVPP V21711)	subadult	0% 19.35 PFB	—	—	—	—	—
Eopengornis (STM24-1)	early subadult	0.9% (38) WB	2.9% 42.4 WB/PFB	1.6% 27 WB/IFLB	—	—	—
Mirarce (UCMP139500)	adult	4.2%*;1.1%* 95.9 PFB/IFLB GL: ~6	—	0.9% 89.0 PFB/FLB GL: 1	1.7%* 48.1 FLB GL: ~6	1.7% 21.7 PFB GL: 1	0.9% 12.2 PFB GL: 3-4
Mirusavis (IVPP V18692)	Adult	0.2% 30.02 PFB GL: 1	—	0.3% 27.33 PFB	—	—	—
Monoenantius (IVPP V20289)	subadult	—	3.5% 45.6 FLB	—	—	—	—
Parapengornis (IVPP V18687)	young subadult	—	—	4.3% 39.8 FLB	—	—	—
Pterygornis (IVPP V16363)	young adult	0.6% 33.5 PFB GL: 1	0.5% 35.4† PFB	0.7% 22.3† PFB	—	—	—
Parvavis (IVPP V18586)	subadult	0.3% 18.4 PFB	—	—	—	—	—
Zhouornis (CNUVB-0908)	Adult	1.6%* 50.6 PFB/CCCB GL: 1	—	0.4% 44.5 PFB GL: 1	—	—	—
STM 29-8	Adult	1.1% 44.7 PFB	—	0.4% 40.2 PFB GL: 2	—	—	—
MACN-S-01	adult	—	—	0%* PFB Gl: 4	—	—	—
PVL-4273	adult	—	—	0.1%* PFB GL: 5	—	—	—

For each element, the following information is given (from top to bottom): measure of approximate vascular porosity (asterisk indicates specimens represented by a fragment of the cortex); measure of total element length, in millimeters (cross indicates estimation); predominant bone tissue for each element (PFB, parallel-fibered bone; WB, woven bone; IFLB, incipient fibrolamellar bone; FLB, fibrolamellar bone; CCCB, compact coarse cancellous bone); and number of growth lines, if present (GL). Measurements of element length are given for the sake of conveying a sense of scale, and reported the most complete side of a given specimen; in some instances (e.g., Mirarce, for which only incomplete elements were destructively sampled) this measurement may not be from the element that was sample.

Monoenantiornis IVPP V20289 (Hu and O'Connor, 2017). This similarity is striking, given the different ontogenetic stages represented by these taxa and differences in the osteohistology of their humeri, suggesting that growth of the radius and ulna slows early in ontogeny relative to other elements in *Mirarce* and other enantiornithines.

Femur

Due to incomplete preservation the left femur was sectioned at the proximal-most portion of the diaphysis (**Figure 3**). Although crushed, the entire circumference of the cortex is represented. The femoral cortex is moderately thick compared to the other elements described here, with a tripartite structure composed of an avascular OCL, a mid-cortical zone of coarse compact cancellous bone (CCCB) and parallel-fibered bone with secondary osteons (expressed variably across the cortex), and an ICL consisting primarily of parallel-fibered bone with lamellar bone present in several regions. Although the OCL is primarily parallel-fibered, lamellar bone tissue is also present in some areas. The medial and cranial cortical portions of the femur are twice as

FIGURE 2 | Histological section through the radius of *Mirarce eatoni*. **(A)** Section showing entire radial fragment sectioned in this study. It is composed of weakly vascularized parallel-fibered bone. 40x, polarized light. White arrow indicates the ICL. **(B)** Close-up of histological section showing details of the growth line (black arrows) and the few vascular channels (white arrows); some are simple canals, while others are incipient or mature primary osteons. 100x, plane light. **(C)** Portion of radial section showing the main and displaced fragments. On the main fragment, the black arrow indicates a growth line. On the displaced fragment, the white arrow indicates the border of the ICL. **(D)** Area in black box of Panel A, an avascular, parellel-fibered region of the radial cortex showing morphological details of the lacunae and fully developed cannaliculi. 400x, plane light. **(E)** Area in white box of panel A, parallel-fibered bone of the radius, showing two incipient primary osteons. 400x, plane light.

thick as the lateral side and are excavated by several large cavities that vary in size and shape, ranging from circular (~50–70 μm diameter) to more elongate and irregular (~180 × 90 μm). These cavities are lined with parallel-fibered or lamellar bone. We posit that these were canals continuous with nutrient foramina open on the surface of the element, where neurovascular bundles passed through the bone. The relatively high concentration of these structures in this section is possibly the result of the proximal diaphyseal location of the sampling (Wang X.-R. et al., 2020).

The texture of the middle cortical layer of the femur varies across the section. CCCB is prominent in the lateral and caudal regions (**Figure 3B,C**), as indicated by the numerous, irregularly shaped structures resembling osteons and the variously-oriented bands of parallel-fibered bone (interstitial lamellae). It is not unexpected to see this tissue type in such abundance given the proximal sampling of the femoral shaft, which represents a former metaphyseal region that later became incorporated into the diaphysis as the femur grew in length (Enlow, 1963) Similarly,

Zhang et al. (2013) report the presence of CCCB in a distally thin-sectioned humerus of *Zhouornis* (CNUVB-0903).

Most of the vasculature in this central region appears to consist of well-developed, longitudinally-oriented channels. Some of these are at the center of secondary osteons in a region of remodeling within the CCCB-dominated caudal portion of the cortex. The cranial and medial portions of the cortex show mainly parallel-fibered matrices, also with secondary osteons. Unlike the humerus, the femur lacks anastomosing vascular canals at the plane of section. The OCL and ICL are avascular. Possibly due to the proximal location of our sample, the vascular area of the femur sample, not including the large cavities in the cortex, is approximately double that of other adult enantiornithine femoral samples (**Table 1**).

Importantly, while the humerus preserves at least six growth lines, only one is visible in the femur. It is located within the inner third of the OCL and only visible in the caudal portion of the cortex. Though this difference might be interpreted as differential
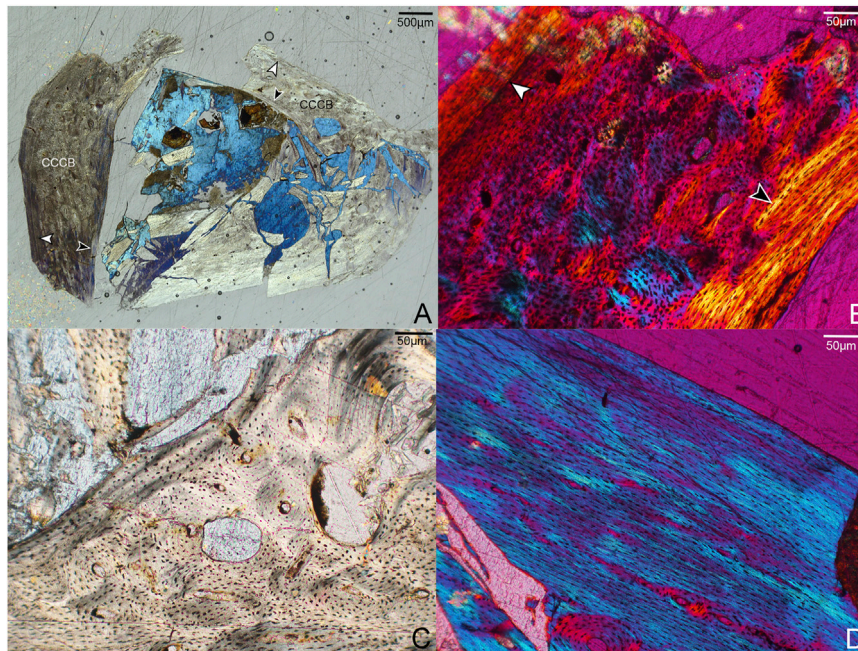
FIGURE 3 | Histological sections through the left femur of *Mirarce eatoni*. **(A)** Section showing entire portion of the left femur; cranial to right, lateral to top. CCCB is widespread in the caudal and lateral regions, closely resembling fibrolamellar bone. Notable are the large cavities in the cranial portion of the cortex. White arrows indicate the OCL; black arrows indicate the ICL. 40x, polarized light. **(B)** Close-up of a portion of the cortex interpreted as CCCB-dominated. The innermost border of the mature ICL is also shown (black arrow). The white arrow indicates a growth line, clearest here in the caudal part of the cortex. 200X, polarized light. **(C)** The large spaces within the cortex, lined with parallel-fibered and lamellar bone. 200x, plane light. **(D)** A parallel-fibered portion of the lateral cortex with low vascular levels. 200x, polarized light.

growth in the fore- and hindlimbs, the proximal position of the section in the femur renders the comparison uncertain. The fact that this structure is only visible in part of the cortex (and not throughout its entire circumference) also speaks to the strong role of cortical drift in the growth and morphological development of the femur. This is similarly suggested by the abundance of CCCB, a tissue type that commonly develops as cortical drift occurs (Heck et al., 2019), in-filling spongy bone to incorporate it into the cortical compacta.

The well-preserved osteocyte lacunae of the femur resemble those in the humerus and other elements in both morphology and distribution. In particular, their organization coincides with differences in bone tissue; bulbous, more-rounded lacunae surrounding primary vascular canals occur in the middle layer of the cortex and grade outward to flattened, circumferentially-aligned lacunae in the OCL.
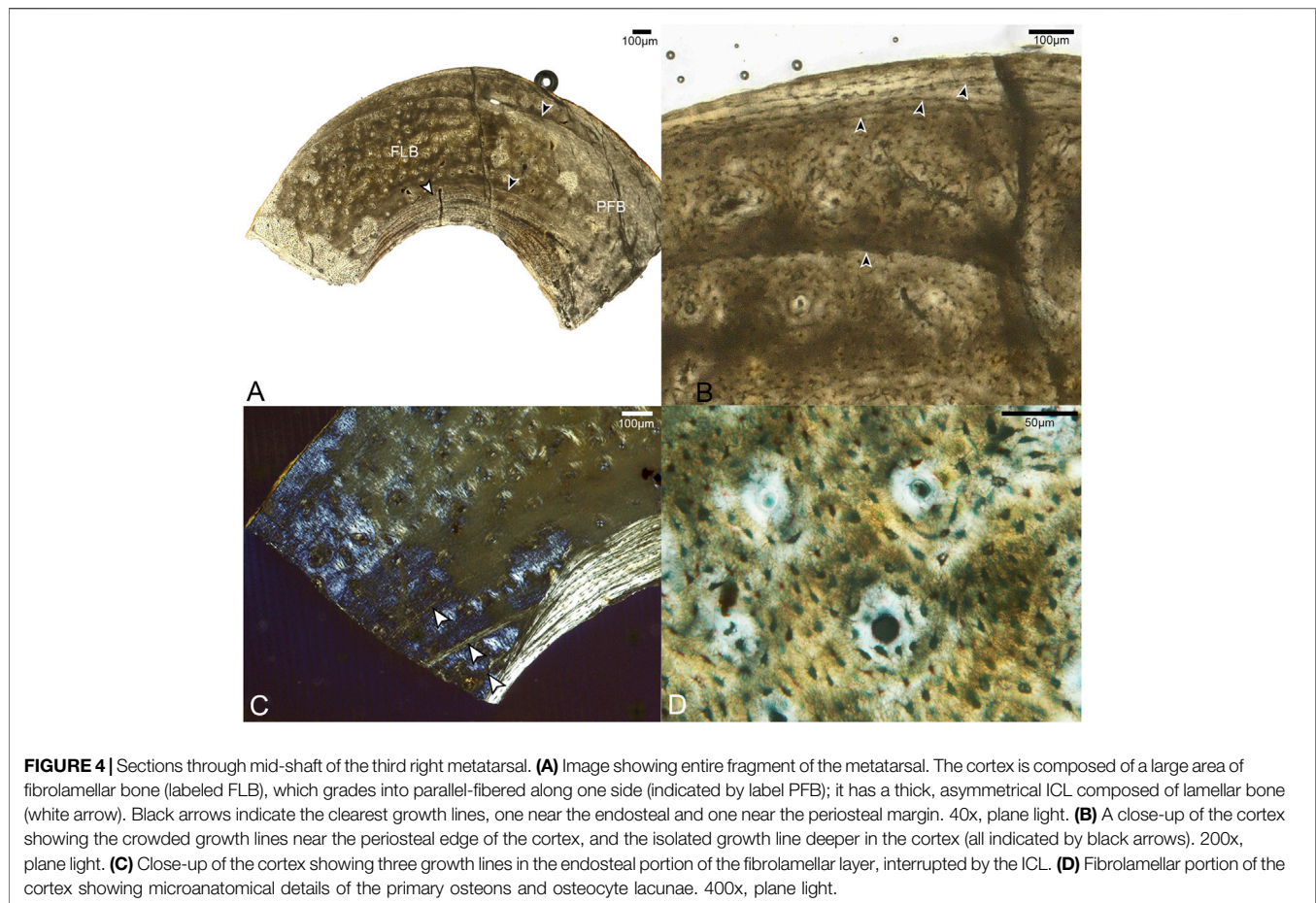
Metatarsal

Samples from the mid-shaft of the third metatarsal were collected from the broken right tarsometatarsus. The fragment captures the entire plantar half of the cortex. The histology is complex, suggesting varying growth rates, bone resorption, and secondary growth. Generally speaking, it is composed of three layers. The cortical bone has a large area of fibrolamellar tissue that grades outward into parallel-fibered along one side, with a thick ICL of endosteally-derived lamellar bone and a thin OCL of parallel-fibered bone (**Figure 4**). In the mid-cortical layer,

osteocyte lacunae are round and disorganized with highly elaborated and fully-developed canalicular systems.

In the OCL, there are 2–3 growth lines, that extend only a short distance around the cortex before terminating at the periosteal margin of the bone. Another growth line is present below the OCL, in the middle cortical layer. All of these are distinctly formed and resemble LAGs. Since the morphology of LAGs and annuli grade into each other, we refrain from specifically labeling these structures. Another three growth lines, resembling annuli, are present near the endosteal margin of the bone. The innermost two run a short course before abruptly ending where they were resorbed by the formation of the ICL, while the third traces a path just outside this structure. The strongly laminated, avascular ICL is widest in the middle of the sampled fragment where it forms approximately 20% the thickness of the bone wall, thinning out laterally and medially. The asymmetry of these structures suggests strong cortical drift occurred during the development of this element, emphasizing the complexity of ontogenetic changes in shaping the tarsometatarsus.

Most of the preserved middle layer of bone is highly vascularized by longitudinal canals, mainly forming the central canals of primary osteons, which populate the fibrolamellar layer in high densities. Some oblique canals are also observed (**Figure 4B**). However, this osteon-dense woven bone grades on one end into a small region of parallel-fibered bone with fewer vascular canals. This further suggests that growth of this element was asymmetrical.

The histological attributes of the metatarsal of *Mirarce* do not closely resemble the metatarsals of *Concornis* LH21006

FIGURE 4 | Sections through mid-shaft of the third right metatarsal. **(A)** Image showing entire fragment of the metatarsal. The cortex is composed of a large area of fibrolamellar bone (labeled FLB), which grades into parallel-fibered along one side (indicated by label PFB); it has a thick, asymmetrical ICL composed of lamellar bone (white arrow). Black arrows indicate the clearest growth lines, one near the endosteal and one near the periosteal margin. 40x, plane light. **(B)** A close-up of the cortex showing the crowded growth lines near the periosteal edge of the cortex, and the isolated growth line deeper in the cortex (all indicated by black arrows). 200x, plane light. **(C)** Close-up of the cortex showing three growth lines in the endosteal portion of the fibrolamellar layer, interrupted by the ICL. **(D)** Fibrolamellar portion of the cortex showing microanatomical details of the primary osteons and osteocyte lacunae. 400x, plane light.

(Cambra-Moo et al., 2006) or *Confuciusornis* NGMC98-8-2 (De Ricqlès et al., 2003) (the only other Cretaceous avians from which metatarsals have been sectioned). In *Confuciusornis* NGMC98-8-2 vascularity is high and the OCL is thin as in *Mirarce*, but compared to *Confuciusornis*, vascularization in *Mirarce* is not exclusively longitudinal in orientation, as some canals show moderate reticulation. In *Concornis* LH21006 the metatarsals are poorly vascularized and consist of a thick cortex of parallel-fibered bone. This stands in contrast to the high vascularity and fibrolamellar texture of the *Mirarce* metatarsal. However, the *Concornis* LH21006 metatarsal section also preserves evidence of remodeling and secondary growth suggesting an early period of rapid growth followed by a major reduction in growth rate as the individual approached somatic maturity. The third metatarsal of *Mirarce* suggests that rapid growth persisted until somatic maturity, only slowing at the time of the formation of the OCL. Nevertheless, we note it is possible that with increased maturity, secondary remodeling comparable to that of *Concornis* LH21006 similarly may have occurred in *Mirarce*.

Pedal Phalanges

Two broken pedal phalanges were sampled at the mid-shaft: the first phalanx of digit II (DIIp1; **Figure 5**) and the fourth phalanx of digit IV (DIVp4; **Figure 6**). The average cortical thickness of

DIIp1 is thinner than that of DIVp4 (**Table 2**). Both pedal phalanges of *Mirarce* are highly vascularized and composed of three distinct layers of tissue: a lamellar ICL of endosteal origin, a middle layer of heavily remodeled bone, and a thin, variably present OCL composed of parallel-fibered bone. In both phalanges, large swaths of the middle are obscured by an expansive, dense Haversian system of longitudinally-oriented secondary osteons (**Figures 5, 6**), with some localized areas of parallel-fibered bone visible. Although difficult to discern due to the degree of remodeling, the bone tissue visible irregularly through the secondary osteons strongly resembles CCCB, with the irregular, wavy occurrences of parallel-fibered bone that presumably were deposited around former trabeculae. Though currently not possible to state with certainty, we posit that the mid-cortical layer of the phalanges was previously dominated by CCCB before undergoing remodeling. This suggests the importance of the role of endosteal resorption, and deposition of secondary endosteal tissue during the shaping and growth of this element. Also, in both phalanges, osteocyte lacunae in the regions of parallel-fibered bone (including in the OCL) are small and flattened. Within the lamellae surrounding the secondary osteons, they are more rounded.

The phalanges were the only elements in this study for which we could examine the complete, uncrushed diaphyseal cross-sections. Notably, there is considerable microanatomical
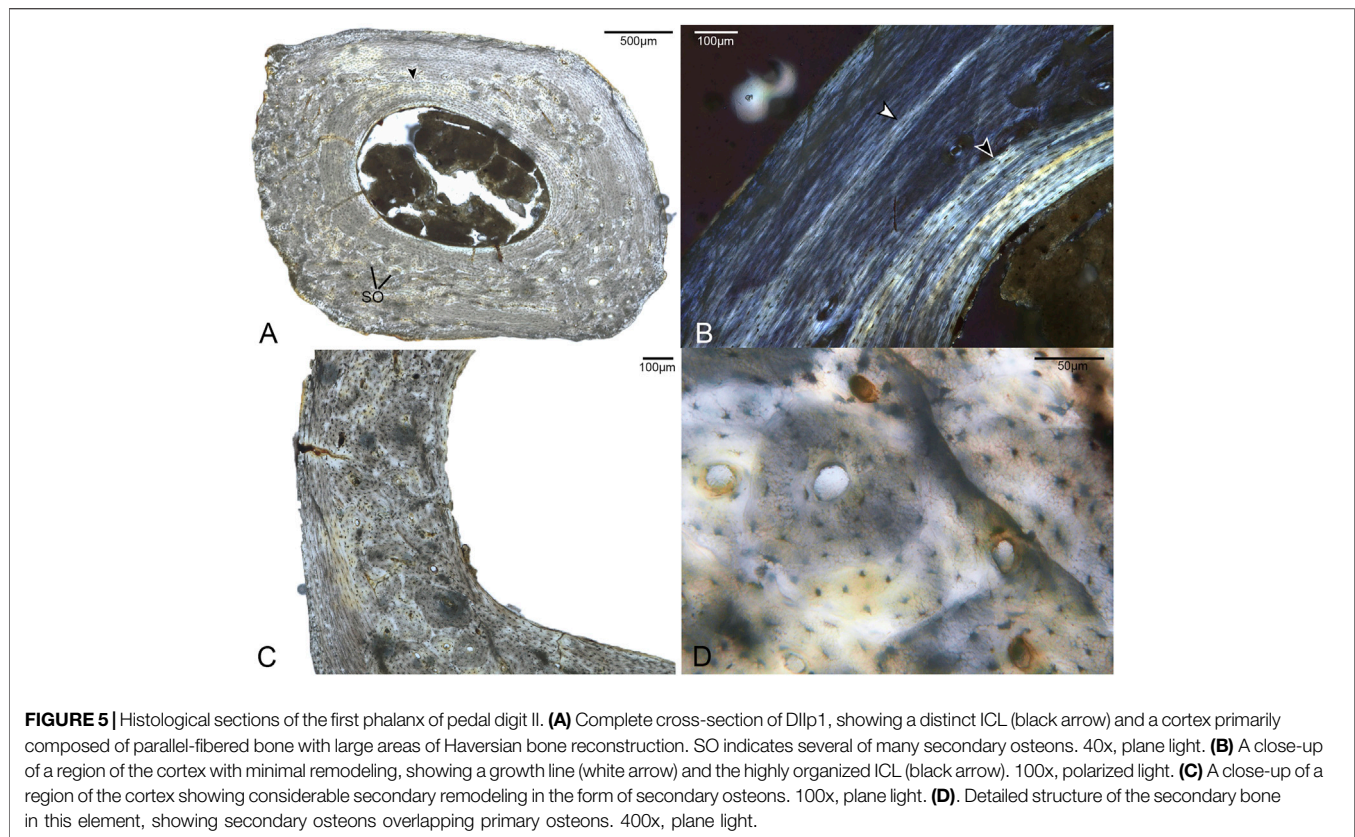
FIGURE 5 | Histological sections of the first phalanx of pedal digit II. **(A)** Complete cross-section of DIIp1, showing a distinct ICL (black arrow) and a cortex primarily composed of parallel-fibered bone with large areas of Haversian bone reconstruction. SO indicates several of many secondary osteons. 40x, plane light. **(B)** A close-up of a region of the cortex with minimal remodeling, showing a growth line (white arrow) and the highly organized ICL (black arrow). 100x, polarized light. **(C)** A close-up of a region of the cortex showing considerable secondary remodeling in the form of secondary osteons. 100x, plane light. **(D)**. Detailed structure of the secondary bone in this element, showing secondary osteons overlapping primary osteons. 400x, plane light.

variation in the cortex of both phalanges (**Figures 5, 6**). Both exhibit a dense clustering of secondary osteons in the medial and lateral regions of the bone, but these gradually become increasingly sparse near the dorsal portion of the cortex. The phalanges were undergoing extensive, asymmetrical remodeling at the time of the individual's death.

While the two phalanges are broadly similar in terms of microanatomy, there are some minor differences. The bone of DIVp4 is generally more organized in terms of osteocyte position and orientation, to the extent that the parallel-fibered bone of the OCL and middle layer border on lamellar (**Figure 6**). There are three to four growth lines present in DIVp4, crowded against the periosteal margin of the bone. Additionally, in DIVp4 the secondary remodeling is more concentrated in the lateral and medial portions of the cortex. In DIIp1 a larger proportion of secondary osteons extend from the medial and lateral cortex into the plantar region, and the mid-cortex is interrupted by a single annulus (**Figure 5**).

DISCUSSION

Enantiornithine life history has been inferred to represent a fairly dramatic departure from relatively rapid growth strategies reported for other Mesozoic stem birds, such as *Confuciusornis* and *Jeholornis* (De Ricqlès et al., 2003; Erickson et al., 2007; Prondvai et al., 2018; Chinsamy et al., 2020). Every previously sampled enantiornithine that can be

considered older than a subadult preserves indications that growth was slow and periodic, as evidenced by a prevalence of parallel-fibered bone. Subsequent studies have revealed higher rates of bone deposition in many enantiornithines across a range of ontogenetic stages compared to that of the first sampled enantiornithines, which revealed avascular parallel fibered bone (Chinsamy and Elzanowski, 2001; Wang M. et al., 2014; Wang X. et al., 2014; Hu et al., 2015; Hu and O'Connor, 2017; Wang et al., 2017a; Knoll et al., 2018), but microanatomy of adult femora still indicates relatively slow growth for a prolonged period of time following reproductive maturity (Zhang et al., 2013; O'Connor et al., 2014; Wang et al., 2017a). The osteohistology of *Mirarce* suggests that at least one lineage of enantiornithines evolved relatively higher growth rates retained later in ontogeny, in the form of intermittent periods of fast post-natal growth in some skeletal elements. However, as in other enantiornithines, growth in *Mirarce* was protracted, as evidenced by the presence of at least six growth lines in the humerus.

The osteohistological variation observed throughout the skeleton of *Mirarce* suggests that, by the Late Cretaceous, some enantiornithine growth strategies evolved to be more nuanced and complex than previously understood. Most major long bone elements in *Mirarce* have a thin, poorly-defined OCL, and the pedal elements show thick, well-developed ICLs. However, beyond these patterns there is considerable microanatomical diversity across the skeleton and the osteohistological characteristics of the middle cortical layers vary greatly. The humerus consists of
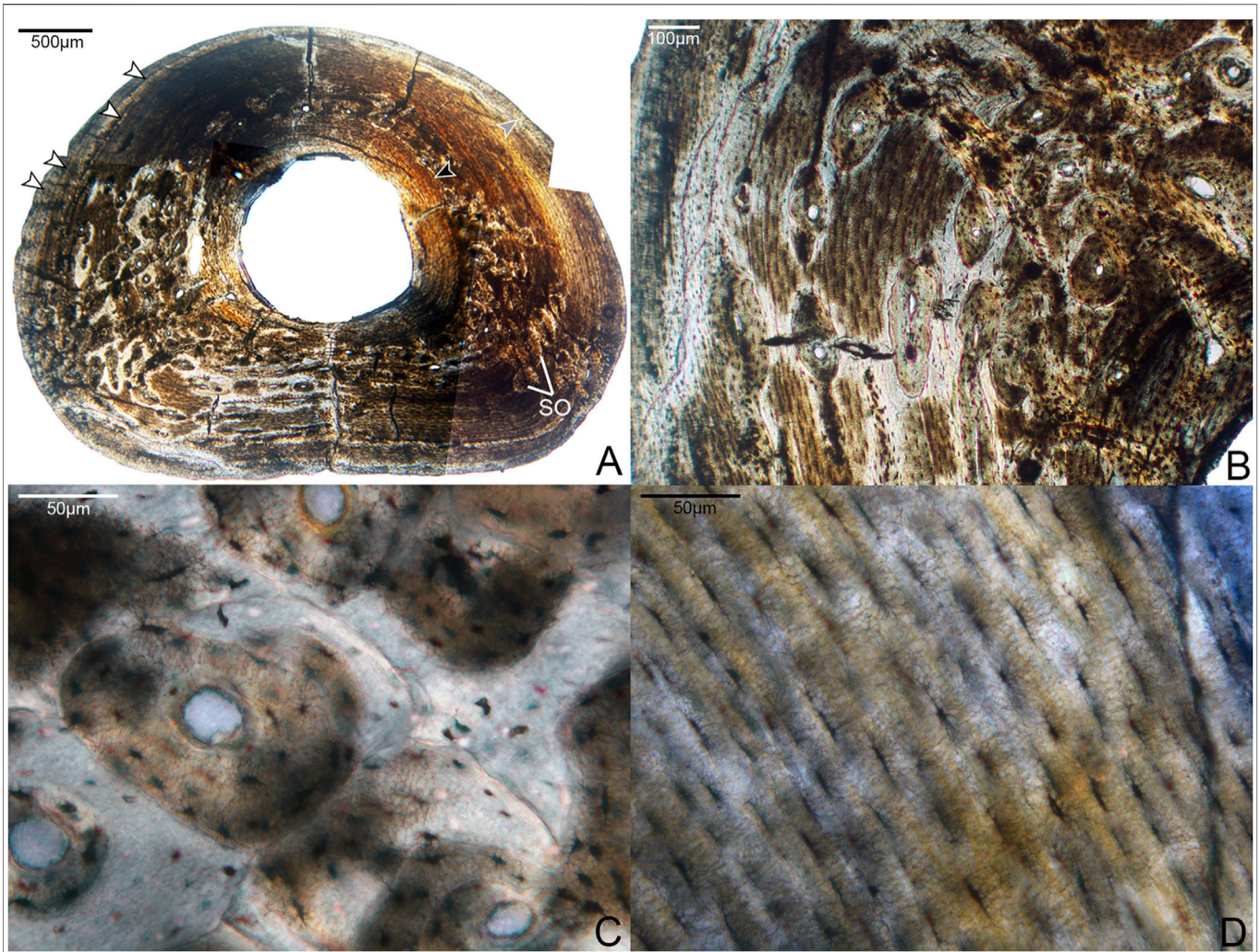
FIGURE 6 | Histological sections of the fourth phalanx of pedal digit IV. **(A)** Complete cross-section of DIVp4, showing a thicker cortex than DIIp2 but otherwise similar organization of tissue: the bone is primarily composed of a parallel-fibered middle layer with large regions of secondary growth, bordered endosteally by a thick, prominent ICL (black arrow) and periosteally by a thin, variably present OCL (gray arrow). White arrows indicate several growth lines, though it is not possible to trace each one entirely around the cortex due to preservational damage. SO indicates several of many secondary osteons. 40x, plane light. **(B)** A close-up of an area of remodeling in the cortex, showing a dense clustering of secondary osteons. 100x; plane light. **(C)** Detailed microanatomy of several secondary osteons present in this element. 400x, plane light. **(D)** Detailed microanatomy of an un-remodeled region of the cortex, composed of parallel-fibered bone with thin, elongate osteocyte lacunae. 400x, plane light.

TABLE 2 | Average cortical diameter and thickness of skeletal elements from *Mirarce eatoni* sectioned in this study.

Element	Average cortical diameter (μm)	Average cortical thickness (μm)
Humerus	—	1542
Femur	5101*	1392
Metatarsal	—	1285
Digit II, phalanx I	1349	766
Digit IV, phalanx IV	2844	1090

Due to the highly fragmentary nature of the sample from the radius, measurements were not taken. Asterisk indicates estimation.

parallel-fibered and regionally distributed incipient fibrolamellar bone, with unusually high vascular porosity (for a skeletally mature enantiornithine) in one humeral thin section (**Table 1**). The radius is entirely parallel-fibered. The femur shows regions of CCCB and parallel-fibered bone, with secondary osteons. The metatarsal is predominantly fibrolamellar with a small parallel-fibered region (although this observation is based on an incomplete cortical cross-section). Finally, the phalanges are regionally parallel-fibered with extensive evidence of remodeling obscuring probable regions of CCCB.

The only other stem-avian taxa for which a comparable breadth of elements has been sampled are the Early Cretaceous *Confuciusornis*, and the Early Cretaceous enantiornithine *Mirusavis*. In the case of *Confuciusornis*, the intraskeletal variation observed in *Mirarce* stands in stark contrast to reported histological patterns (De Ricqlès et al., 2003; Chinsamy et al., 2020). *Confuciusornis* exhibits fibrolamellar bone and high levels of vascularity nearly uniformly across all sectioned elements (including the same elements as were sampled in this study). This demonstrates that, although both the *Mirarce* and *Confuciusornis* lineages had relatively elevated growth rates, each lineage was characterized by very different growth strategies, thereby producing very different osteohistological features across the skeleton. Overall, growth in *Confuciusornis* is more similar to that in crown birds, reaching near adult size within the first year such that all LAGs are located in the OCL (De Ricqlès et al., 2003; Chinsamy et al., 2020), whereas elevated bone deposition rates in *Mirarce* were interrupted numerous times prior to achieving skeletal maturity as evidenced by growth lines located within the inner portion of the bone cortex.

The Early Cretaceous enantiornithine *Mirusavis* has also been sampled nearly as extensively as *Mirarce*, with five elements sectioned (humerus, radius, femur, tibiotarsus and scapula) and the entire specimen scanned using computed tomography (Wang M. et al., 2020). The distal hindlimbs are not preserved in *Mirusavis* such that comparison with *Mirarce* can only be made between the humerus, radius, and femur. In contrast to *Mirarce*, the histology in all long bone elements of *Mirusavis* is very consistent, with all sampled cortices composed of parallel fibered bone with little to no vascularization, which consists of simple longitudinal canals where present (Wang M. et al., 2020). The computed tomography scans suggest this bone tissue predominated throughout the entire preserved skeleton. A single LAG is present in the humerus and tibiotarsus but no growth lines are visible in either the radius or femur. Compared to *Mirarce*, growth in *Mirusavis* appears to have been far more consistent between elements. The absence of any indication of remodeling may be due to the relatively more immature ontogenetic stage of this taxon, which was likely still growing despite the fact it was clearly reproductively active, as indicated by the preservation of medullary bone (Wang M. et al., 2020).

While the radius of *Mirarce* exhibits histological characteristics that have come to be expected for enantiornithines (a cortex predominantly composed of parallel-fibered bone with low vascular porisity), other elements of this taxon preserve the first evidence of fibrolamellar/incipient fibrolamellar bone tissue in a somatically mature enantiornithine. This tissue type was previously only known in a perinatal enantiornithine specimen (Chinsamy and Elzanowski, 2001). Although growth rates were apparently not as elevated as those observed in *Confuciusornis* and some ornithuromorphs [e.g., *Iteravis* and *Ichthyornis* (Chinsamy et al., 1998; O'Connor et al., 2015)] the incipient fibrolamellar bone in the humerus and fibrolamellar complex in the tarsometatarsus of *Mirarce* are unique among enantiornithines, thereby increasing the recognized diversity of developmental strategies utilized by this clade.

The humerus of *Mirarce* exhibits a complex and variegated growth pattern. The endosteal and periosteal layers of organized, parallel-fibered bone, together with the growth lines in each of these layers, is indicative of a sustained period of slow growth. The middle layer of incipient fibrolamellar bone in the humerus suggests that this was interrupted by a period of rapid growth. These data reveal a cyclical growth strategy, with a period of slow growth followed by a period of faster growth, and then culminating with a resumption of slow growth. In the OCL, the more numerous growth lines, separated by smaller spaces suggests that this second slowing of growth was more prolonged. It is possible there were additional cycles of slow and fast growth, the traces of which may have been erased by endosteal resorption. This pattern stands in contrast to other enantiornithine taxa, which have humeri with very low levels of vascularity and cortices composed of parallel-fibered bone with either no LAG expression (*Mirusavis* IVPP V18962 (Wang M. et al., 2020), *Parvavis* IVPP V18586 (Wang M. et al., 2014), *Cruralispennia* IVPP V21711 (Wang et al., 2017b), *Pterygornis* IVPP V16363 (Wang et al., 2017a)) or with LAGs in the mid-cortex (STM29-8 (O'Connor et al., 2014)). The overall absence of fibrolamellar bone in these enantiornithines suggest that rapid growth ceased at a much earlier stage in postnatal development. This may also be partially due to differences in body size, since Early Cretaceous enantiornithines were overall much smaller. However, variation in body size cannot explain differences in bone tissue observed between *Mirarce* and similarly sized enantiornithines from the Late Cretaceous Lecho Formation in which the cortical bone consists entirely of avascular parallel-fibered tissue (Chinsamy et al., 1995).

The tarsometatarsus of *Mirarce* shows evidence of a similar cyclical pattern. The middle cortical layer is dominated by fibrolamellar bone, bounded by an OCL containing 2-3 growth lines. There is also evidence of three growth lines in the endosteal portion of the middle layer, that have been partially obscured by endosteal resorption and deposition of the ICL. None of the growth lines present in this element can be traced for any great distance around the cortex, indicating strong cortical drift and asymmetrical growth. This asymmetrical growth is also hinted at by a small parallel-fibered area, which possibly was part of a larger region of this element that was growing more slowly than the portion sectioned in this study. Evidence of asymmetrical growth similarly occurs in the femur, with CCCB concentrated in the lateral and caudal regions. The single growth mark (visible only in the caudal cortex due to cortical drift) is located near the periosteal surface. This element exhibits an OCL, ICL, and middle cortical layer with no additional evidence of the cycles of slow and fast growth seen in the humerus and metatarsal.

The surprising difference in number of growth lines between the femur and the humerus could be accounted for in several ways. If the skeleton was indeed exposed subaerially, lines could have been lost due to flaking. However, our examination of the exterior bone of the femur rules out significant loss of external cortex. The more proximal position of the femoral sample provides a possible alternate explanation. Ossification of avian long bones proceeds from the midshaft, so the more proximal sample might potentially preserve fewer growth marks. However,

if this were the case, one would expect the recovered LAGs in the proximal sample to be the most external, which is not the case here. Another alternative is that additional LAGs were lost due to periosteal resorption, consistent with the evidence of strong cortical drift in the femur. Ultimately, at this juncture we can only suggest that a better understanding of the possibility of differential timing in enantiornithine forelimb/hindlimb development requires additional data.

Taken collectively, these data support previous inferences that enantiornithines did not experience extended periods of very fast, sustained skeletal growth in which skeletal maturity was achieved within the first year as in most modern birds. However, it is not entirely accurate to characterize this entire clade as "slow growing." Evidence from *Mirarce* indicates that, by the Late Cretaceous, at least one lineage of enantiornithines evolved relatively higher growth rates that were periodically sustained to varying degrees across the skeleton into later ontogenetic stages. Some elements matured very early in ontogeny (the radius); others continued fast growth intermittently into adulthood (the humerus and tarsometatarsus); and still others document high levels of secondary growth and remodeling (the pedal phalanges and portions of the femur). The variation observed in this taxon indicates allometric growth between different elements. This has already been observed in previous studies of both ornithuromorphs and some enantiornithines, in which the pectoral limb elements consistently show signs indicative of faster growth compared to the pelvic limb (O'Connor et al., 2014; Wang and Zhou, 2016). Such allometric growth has similarly been documented in Neornithes (e.g., Carrier and Auriemma, 1992; Prondvai et al., 2020).

Enantiornithine Life History Patterns

Observations from this study allow us to hypothesize several life history trends across Enantiornithes. First, antebrachial elements (the radius and ulna) in adult and late-subadult individuals are almost exclusively characterized by slow-growing bone across taxa and even ontogenetic stages. More generally speaking, these elements are often composed of bone that is more mature relative to the humerus (with a greater proportion of parallel-fibered bone, lower vascularity, and in some cases even lamellar bone). This is the case in *Mirarce*, *Pterygornis* IVPP V16363 (Wang et al., 2017a), subadult *Eopengornis* STM24-1 (Wang X. et al., 2014), and *Mirusavis* IVPP V18692 (Wang M. et al., 2020). The differences in humeral growth may produce ontogenetic differences in the proportions of the forelimb elements (such that the humerus is relatively shorter in juveniles) that reflect phylogenetic underpinnings (the relatively shorter humerus in non-avian non-volant close relatives). Further analyses of enantiornithine intraskeletal variation across ontogenetic stages, and quantitative assessments of histological maturity, will help parse out answers to these questions of function.

Furthermore, a difference in "maturity" of the humerus and femur also appears to be a common characteristic of the clade Enantiornithes. The humerus often exhibits bone that is less mature and faster growing than the femur, being characterized by relatively higher levels of vascularity, the presence of regional incipient fibrolamellar bone (in some cases), a comparatively less-developed OCL, and/or and fewer growth lines. Femora, in contrast, often have lower vascularity, no fibrolamellar bone, thicker OCLs, and more growth lines. This pattern persists in most enantiornithines for which the humerus and femur have both been sectioned (e.g., *Zhouornis* CNUVB-0903 (Zhang et al., 2013), STM 29-8 (O'Connor et al., 2014), *Pterygornis* IVPP V16363 (Wang et al., 2017a), and *Eopengornis* STM24-1 (Wang X. et al., 2014)). Furthermore, Prondvai et al. (2018) assign higher "intraskeletal precocity ranks" to the humerus than the femur in *Eosinopteryx*, *Anchiornis*, and *J. curvipes*; that is, they describe the tissue of the humerus as less functionally mature than that of the femur. Additionally, the humerus was found to be less mature than pelvic limb elements in the dromaeosaurid dinosaurs *Wulong* and *Sinornithosaurus* (Poust et al., 2020). The seemingly widespread occurrence of this pattern suggests it may have deep evolutionary origins.

However, we note that *Mirusavis* appears to break from this larger trend, exhibiting a growth line in the humerus and not the femur. Furthermore, whether *Mirarce* holds to this pattern is currently ambiguous. In terms of certain attributes, the humerus does indeed bear evidence of being faster-growing (e.g., reticulating canals, higher vascular porosity, and regional fibrolamellar bone). On the other hand, this bone has considerably more growth lines than the femur, suggesting that growth of this element had slowed down much earlier. The proximal sampling of the femur and incomplete cross-section of the humeral cortex make meaningful comparisons difficult. This will remain an open question until potential non-destructive histological analysis of the complete humerus and femur of the holotype can be conducted or more specimens become available through future collecting. This question also emphasizes the need for additional histological sectioning of other large-bodied Mesozoic birds.

CONCLUSION

The microanatomy of *Mirarce eatoni* is complex and highly variable both across the skeleton, and even within individual elements. This specimen emphasizes that many categories used to describe microstructural anatomy are in fact part of a spectrum. Fibrolamellar bone may be incipient and may grade into parallel-fibered tissue. Orientation of vascular canals may be predominantly reticular in one thin section, and predominantly longitudinal in the consecutive section. A LAG may grade into an annulus, forming a growth line that is not definitively one or the other. A cross-section of a single element may have large regions of fast-growing bone and large regions of slower-growing bone, leading to asymmetrical growth and the formation of anatomical landmarks at the gross level.

Some skeletal elements of *Mirarce eatoni*, such as the radius, underwent relatively constant, slow growth. Others underwent alternating periods of slow and fast growth, as indicated in the histological patterns of the humerus and tarsometatarsus. Still

others, such as the femur and phalanges, underwent extensive secondary remodeling. Some elements also indicate that asymmetrical growth was an important strategy for achieving adult morphology in this taxon, as seen in the tarsometatarsus and femur. This very possibly was even more common across the skeleton, though our data here are limited by the necessity of sampling only broken bones in the holotype specimen.

This growth strategy appears to represent a marked departure from that of other enantiornithines, which generally appear to have been dominated by slow, steady growth occasionally slowing enough to deposit a growth line. These differences may be partially attributable to body size; *Mirarce* is considerable larger than most of the small, Early Cretaceous enantiornithines that have been sampled. However, it is significant that *Mirarce* also appears to differ substantially from other large-bodied, Late Cretaceous enantiornithines (Chinsamy et al., 1995), although this may be a result of differences in sampling location, as we were forced to sample the femoral diaphysis proximally.

Additional intraskeletal sampling of other enantiornithines may reveal that the ontogenetic patterns of *Mirarce* were more common in this clade or may provide additional evidence that these are derived traits of the Late Cretaceous taxon. Ultimately, this study emphasizes the importance of understanding intraskeletal patterns of ontogeny by sampling multiple elements and using this as a basis for making inferences about growth strategies and life-history traits.

DATA AVAILABILITY STATEMENT

The datasets presented in this study can be found in online repositories. The names of the repository/repositories and accession number(s) can be found below: Photographs of histological sections of the specimens presented in this paper (both those used in the figures and additional images) are available from Zenodo (https://zenodo.org). The original thin-sections can be accessed at the University of California Museum of Paleontology in Berkeley, CA, United States.

REFERENCES

Atterholt, J., Hutchison, J. H., and O'Connor, J. K. (2018). The most complete enantiornithine from North America and a phylogenetic analysis of the Avisauridae. *PeerJ* 6, e5910. doi:10.7717/peerj.5910

Bourdon, E., Castanet, J., de Ricqlès, A., Scofield, P., Tennyson, A., Lamrous, H., et al. (2009). Bone growth marks reveal protracted growth in New Zealand kiwi (Aves, Apterygidae). *Biol. Lett.* 5, 639–642. doi:10.1098/rsbl.2009.0310

Cambra-Moo, O., Buscalioni, Á. D., Cubo, J., Castanet, J., Loth, M.-M., De Margerie, E., et al. (2006). Histological observations of enantiornithine bone (saurischia, Aves) from the lower cretaceous of las hoyas (Spain). *Comptes Rendus Palevol* 5, 685–691. doi:10.1016/j.crpv.2005.12.018

Carrier, D. R., and Auriemma, J. (1992). A developmental constraint on the fledging time of birds. *Biol. J. Linn. Soc.* 47, 1–17. doi:10.1111/j.1095-8312.1992.tb00656.x

Chinsamy, A., and Elzanowski, A. (2001). Bone histology. Evolution of growth pattern in birds. *Nature* 412, 402. doi:10.1038/35086650

Chinsamy, A., Marugán-Lobón, J., Serrano, F. J., and Chiappe, L. (2020). Osteohistology and life history of the basal pygostylian, *Confuciusornis sanctus*. *Anat. Rec. (Hoboken)* 303, 949–962. doi:10.1002/ar.24282

Chinsamy, A., Chiappe, L. M., and Dodson, P. (1995). Mesozoic avian bone microstructure: physiological implications. *Paleobiology* 21, 561–574. doi:10.1017/s0094837300013543

Chinsamy-Turan, A. (2005). *The microstructure of dinosaur bone: deciphering biology with fine-scale techniques*. Baltimore: John Wiley & Sons.

Cullen, T. M., Canale, J. I., Apesteguía, S., Smith, N. D., Hu, D., and Makovicky, P. J. (2020). Osteohistological analyses reveal diverse strategies of theropod dinosaur body-size evolution. *Proc. Biol. Sci.* 287, 20202258. doi:10.1098/rspb.2020.2258

Cullen, T. M., Evans, D. C., Ryan, M. J., Currie, P. J., and Kobayashi, Y. (2014). Osteohistological variation in growth marks and osteocyte lacunar density in a

theropod dinosaur (Coelurosauria: ornithomimidae). *BMC Evol. Biol.* 14, 231. doi:10.1186/s12862-014-0231-y

De Ricqlès, A. J., Padian, K., Horner, J. R., Lamm, E.-T., and Myhrvold, N. (2003). Osteohistology of *Confuciusornis sanctus*(theropoda: Aves). *J. Vertebr. Paleontol.* 23, 373. doi:10.1671/0272-4634(2003)023[0373: oocsta]2.0.co;2

De Ricqlès, A. (1976). "On bone histology of fossil and living reptiles, with comments on its functional and evolutionary significance," in *Morphology and biology of reptiles*. Editor C. B. Cox. London, United Kingdom: Linnean Society, 123–149.

Enlow, D. H. (1963). *Principles of bone remodeling: an account of post-natal growth and remodeling processes in long bones and the mandible.* Springfield: Generic.

Erickson, G. (2005). Assessing dinosaur growth patterns: a microscopic revolution. *Trends Ecol. Evol. (Amst)* 20, 677–684. doi:10.1016/j.tree. 2005.08.012

Erickson, G. M., Curry Rogers, K., Varricchio, D. J., Norell, M. A., and Xu, X. (2007). Growth patterns in brooding dinosaurs reveals the timing of sexual maturity in non-avian dinosaurs and genesis of the avian condition. *Biol. Lett.* 3, 558–561. doi:10.1098/rsbl.2007.0254

Erickson, G. M., Rauhut, O. W., Zhou, Z., Turner, A. H., Inouye, B. D., Hu, D., et al. (2009). Was dinosaurian physiology inherited by birds? Reconciling slow growth in *Archaeopteryx. PLoS One* 4, e7390. doi:10.1371/ journal.pone.0007390

Evans, D. C., Barrett, P. M., Brink, K. S., and Carrano, M. T. (2015). Osteology and bone microstructure of new, small theropod dinosaur material from the early Late Cretaceous of Morocco. *Gondwana Res.* 27, 1034–1041. doi:10.1016/j.gr. 2014.03.016

Francillon-Vieillot, H., De Buffrénil, V., Castanet, J., Géraudie, J., Meunier, F., Sire, J., et al. (1990). "Microstructure and mineralization of vertebrate skeletal tissues," in *Skeletal biomineralization: patterns, processes, and evolutionary trends*. Editor J. G. Carter. New York, NY: Van Nostrand Reinhold, 471–530.

Gill, F. B. (2007). "Parents and their offspring," in *Ornithology*. Editor F. B. Gill.. 3rd Edition (New York, NY: WH Freeman and Company), 467–502.

Heck, C. T., Varricchio, D. J., Gaudin, T. J., Woodward, H. N., and Horner, J. R. (2019). Ontogenetic changes in the long bone microstructure in the nine-banded armadillo (*Dasypus novemcinctus*). *PLoS One* 14, e0215655. doi:10. 1371/journal.pone.0215655

Horner, J. R., De Ricqlès, A., and Padian, K. (2000). Long bone histology of the hadrosaurid dinosaur*Maiasaura peeblesorum*: growth dynamics and physiology based on an ontogenetic series of skeletal elements. *J. Vertebr. Paleontol.* 20, 115–129. doi:10.1671/0272-4634(2000)020 [0115:lbhoth]2.0.co;2

Horner, J. R., de Ricqlès, A., and Padian, K. (1999). Variation in dinosaur skeletochronology indicators: implications for age assessment and physiology. *Paleobiology* 25, 295–304. doi:10.1017/s0094837300021308

Hu, H., O'Connor, J. K., and Zhou, Z. (2015). A new species of Pengornithidae (Aves: Enantiornithes) from the Lower Cretaceous of China suggests a specialized scansorial habitat previously unknown in early birds. *PLoS One* 10, e0126791. doi:10.1371/journal.pone.0126791

Hu, H., and O'connor, J. K. (2017). First species of Enantiornithes from Sihedang elucidates skeletal development in Early Cretaceous enantiornithines. *J. Syst. Palaeontology* 15, 909–926. doi:10.1080/ 14772019.2016.1246111

Huttenlocker, A. K., Woodward, H. N., and Hall, B. K. (2013). "The biology of bone," in *Bone histology of fossil tetrapods*. Editors K. Padian and E.-T. Lamm. Berkeley and Los Angeles: University of California Press, 13–34.

Knoll, F., Chiappe, L. M., Sanchez, S., Garwood, R. J., Edwards, N. P., Wogelius, R. A., et al. (2018). A diminutive perinate European Enantiornithes reveals an asynchronous ossification pattern in early birds. *Nat. Commun.* 9, 937–939. doi:10.1038/s41467-018-03295-9

Lee, A. H., and Werning, S. (2008). Sexual maturity in growing dinosaurs does not fit reptilian growth models. *Proc. Natl. Acad. Sci. USA* 105, 582–587. doi:10. 1073/pnas.0708903105

Lee, A. H., and O'Connor, P. M. (2013). Bone histology confirms determinate growth and small body size in the noasaurid theropod*Masiakasaurus*

knopfleri. *J. Vertebr. Paleontol.* 33, 865–876. doi:10.1080/02724634.2013. 743898

O'Connor, J. K., Chiappe, L. M., and Bell, A. (2011). "Pre-modern birds: avian divergences in the mesozoic," in *Living dinosaurs: the evolutionary history of modern birds*. Editors G. Dyke and G. Kaiser (New York, NY: John Wiley & Sons, Ltd.), 39–114.

O'Connor, J. K., Erickson, G. M., Norell, M., Bailleul, A. M., Hu, H., and Zhou, Z. (2018). Medullary bone in an Early Cretaceous enantiornithine bird and discussion regarding its identification in fossils. *Nat. Commun.* 9, 1–8. doi:10.1093/nsr/nwz214

O'Connor, J. K., Wang, M., Zheng, X.-T., Wang, X.-L., and Zhou, Z.-H. (2014). The histology of two female Early Cretaceous birds. *Vertebrata PalAsiatica* 52, 112–128.

O'Connor, J. K., Wang, M., Zhou, S., and Zhou, Z. (2015). Osteohistology of the lower cretaceous yixian formation ornithuromorph (Aves) *Iteravis huchzermeyeri. Palaeontol. Electronica* 18, 1–11. doi:10.26879/520

Poust, A. W., Gao, C., Varricchio, D. J., Wu, J., and Zhang, F. (2020). A new microraptorine theropod from the Jehol Biota and growth in early dromaeosaurids. *Anat. Rec. (Hoboken)* 303, 963–987. doi:10.1002/ar. 24343

Prondvai, E., Witten, P. E., Abourachid, A., Huysseune, A., and Adriaens, D. (2020). Extensive chondroid bone in juvenile duck limbs hints at accelerated growth mechanism in avian skeletogenesis. *J. Anat.* 236, 463–473. doi:10.1111/joa. 13109

Prondvai, E., Godefroit, P., Adriaens, D., and Hu, D.-Y. (2018). Intraskeletal histovariability, allometric growth patterns, and their functional implications in bird-like dinosaurs. *Scientific Rep.* 8, 1–16. doi:10.1038/ s41598-018-20640-6

Wang, M., Li, Z., and Zhou, Z. (2017a). Insight into the growth pattern and bone fusion of basal birds from an Early Cretaceous enantiornithine bird. *Proc. Natl. Acad. Sci. USA* 114, 11470–11475. doi:10.1073/pnas. 1707237114

Wang, M., O'Connor, J. K., Pan, Y., and Zhou, Z. (2017b). A bizarre Early Cretaceous enantiornithine bird with unique crural feathers and an ornithuromorph plough-shaped pygostyle. *Nat. Commun.* 8, 1–12. doi:10. 1038/ncomms14141

Wang, M., O'Connor, J. K., Bailleul, A. M., and Li, Z. (2020). Evolution and distribution of medullary bone: evidence from a new Early Cretaceous enantiornithine bird. *Natl. Sci. Rev.* 7, 1068–1078. doi:10.1093/nsr/ nwz214

Wang, X.-R., Cau, A., Kundrát, M., Chiappe, L. M., Ji, Q., Wang, Y., et al. (2020). A new advanced ornithuromorph bird from Inner Mongolia documents the northernmost geographic distribution of the Jehol paleornithofauna in China. *Hist. Biol.*. doi:10.1080/08912963.2020.1731805

Wang, M., and Zhou, Z. (2016). A new adult specimen of the basalmost ornithuromorph bird *Archaeorhynchus spathula* (Aves: Ornithuromorpha) and its implications for early avian ontogeny. *J. Syst. Palaeontology* 15, 1–18. doi:10.1080/14772019.2015.1136968

Wang, M., Zhou, Z., and Xu, G. (2014). The first enantiornithine bird from the Upper Cretaceous of China. *J. Vertebr. Paleontol.* 34, 135–145. doi:10.1080/ 02724634.2013.794814

Wang, X., O'Connor, J. K., Zheng, X., Wang, M., Hu, H., and Zhou, Z. (2014). Insights into the evolution of rachis dominated tail feathers from a new basal enantiornithine (Aves: ornithothoraces). *Biol. J. Linn. Soc. Lond.* 113, 805–819. doi:10.1111/bij.12313

Werning, S. (2012). The ontogenetic osteohistology of *Tenontosaurus tilletti. PLoS One* 7, e33539. doi:10.1371/journal.pone.0033539

Woodward, H. N., Horner, J. R., and Farlow, J. O. (2014). Quantification of intraskeletal histovariability in Alligator mississippiensis and implications for vertebrate osteohistology. *PeerJ* 2, e422. doi:10.7717/peerj.422

Xu, X., Zhou, Z., Dudley, R., Mackem, S., Chuong, C. M., Erickson, G. M., et al. (2014). An integrative approach to understanding bird origins. *Science* 346, 1253293. doi:10.1126/science.1253293

Zhang, F., Hou, L., and Ouyang, L. (1998). Osteological microstructure of *Confuciusornis*: preliminary report. *Vertebrata PalAsiatica* 36, 126–135.

Zhang, Z., Chiappe, L. M., Han, G., and Chinsamy, A. (2013). A large bird from the Early Cretaceous of China: new information on the skull of

enantiornithines. *J. Vertebr. Paleontol.* 33, 1176-1189. doi:10.1080/02724634.2013.762708

Zheng, X., O'Connor, J., Wang, X., Wang, M., Zhang, X., and Zhou, Z. (2014). On the absence of sternal elements in *Anchiornis* (Paraves) and *Sapeornis* (Aves) and the complex early evolution of the avian sternum. *Proc. Natl. Acad. Sci. USA* 111, 13900–13905. doi:10.1073/pnas.1411070111

Zheng, X., O'connor, J. K., Wang, X., Pan, Y., Wang, Y., Wang, M., et al. (2017). Exceptional preservation of soft tissue in a new specimen of *Eoconfuciusornis* and its biological implications. *Natl. Sci. Rev.* 4, 441–452. doi:10.1093/nsr/nwx004

GLOSSARY

CNU Capital Normal University, Beijing, China

IVPP Institute of Paleontology and Paleoanthropology, Beijing, China

LH Las Hoyas Collection, Unidad de Paleontología, Universidad Autonóma de Madrid, Madrid, Spain

MACN Seccíon Paleontología de Vertebrados, Museo Argentino de Ciencias Naturales, Buenos Aires, Argentina

MPCM Museo de Paleontología de Castilla-La Mancha, Cuenca, Spain

NGMC National Geological Museum, Beijing, China

PVL Fundación Instituto Miguel Lillo, Tucumán, Argentina

STM Shandong Tianyu Museum of Nature, Pingyi, China

UCMP University of California Museum of Paleontology, Berkeley, United States

ZPAL Zoological Institute of Palaeobiology of the Polish Academy of Sciences, Warsaw, Poland